The Jovian ionospheric conductivity derived from a broadband precipitated electron distribution

G. Sicorello[1], B. Bonfond[1], J.-C. Gérard[1], D. Grodent[1], L. Gkouvelis[2], G.R. Gladstone[3,4] and A. Salveter[5]

[1]ULiège (Belgium), [2]LMU München (Germany), [3]SwRI (Texas), [4]UTSA (Texas), [5]UoC (Germany)

Contact: guillaume.sicorello@uliege.be

This presentation participates in OSPP

Outstanding Student & PhD candidate Presentation contest

In a nutshell

- The conductivity at Jupiter is almost always computed assuming a simple mono-energetic auroral electron precipitation at high latitudes.
- The effect of a more realistic broadband electron distribution on the conductivity is investigated.
- Our model shows that mono-energetic distributions either overestimate (up to 1.6-fold) or underestimate (up to 10-fold) the conductance, depending on the mean energy of the precipitating electrons.

1. Introduction

The **Pedersen ionospheric conductivity and conductance** at Jupiter are key elements when considering the exchange of momentum and energy between the ionosphere and the magnetosphere.
Most models assume a **mono-energetic** distribution to represent the electron flux (e.g. Gérard *et al.*, 2020). However, based on the recent findings from the Juno spacecraft, it appears that the impinging electron distribution is best approximated with a **broadband** distribution (e.g. Mauk *et al.*, 2017; Salveter *et al.*, 2022). **What are the effects of such a distribution on the conductivity/conductance?**

2. Ionospheric model

The ionospheric model presented in Gérard *et al.* (2020) is adopted:

- Altitude distributions of **H**, $\mathbf{H_2}$ and $\mathbf{CH_4}$ taken from Grodent *et al.* (2001) model.
- Above the homopause, conductivity mainly driven by the $\mathbf{H_3^+}$ **ion**:

$$H_2^+ + H_2 \longrightarrow H_3^+ + H.$$

- Close to and below the homopause, rapid reaction of CH_4 with H_3^+ produces **hydrocarbon ions** responsible for the conductivity. $\mathbf{CH_5^+}$ is considered as the main hydrocarbon product (Wang *et al.*, 2021):

$$H_3^+ + CH_4 \longrightarrow CH_5^+ + H_2.$$

- H_2^+ profile computed using the formulation given by Hiraki & Tao (2008).

3. Conductivity σ_P and conductance Σ_P

$$\sigma_P = e^2 n_e \left[\frac{\nu_{en}}{m_e(\nu_{en}^2 + \omega_e^2)} + \sum_i \frac{\nu_{in}}{m_i(\nu_{in}^2 + \omega_i^2)} \right], \qquad \Sigma_P = \int \sigma_P dz.$$

- e: electron charge.
- $\nu_{en}(\nu_{in})$: electron (ion)-neutral collision frequency.
- $m_e(m_i)$: electron (ion) mass.
- $\omega_e(\omega_i)$: electron (ion) gyrofrequency.
- z: altitude.

4. Kappa distribution

The kappa function f is chosen to model the broadband shape of the electron energy distribution (Coumans *et al.*, 2002). It is defined by the **total energy flux** Q_0 (unit: mW.m^{-2}), the **mean energy** $\langle E \rangle$ (unit: keV) and an additionnal parameter κ describing the high energy tail of the distribution:

$$f(E) = \frac{4Q_0}{\pi} \frac{\kappa(\kappa-1)}{(\kappa-2)^2} \frac{E}{\langle E \rangle} \frac{\langle E \rangle^{\kappa-1}}{\left(\frac{2E}{\kappa-2} + \langle E \rangle\right)^{\kappa+1}}$$

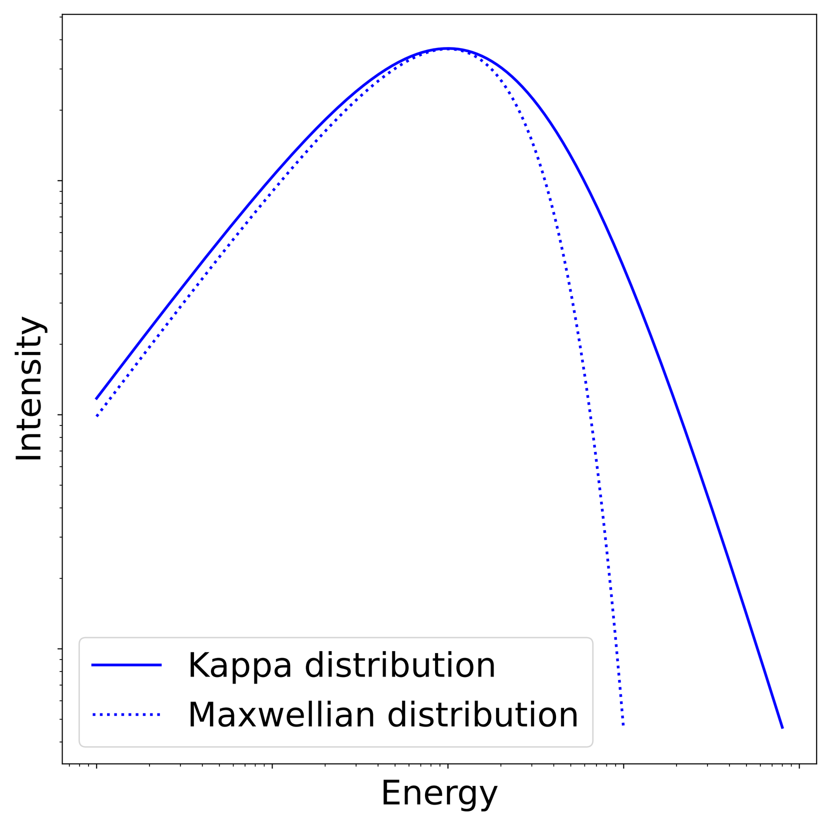

Fig. 1: Representation of a **maxwellian and a kappa distributions** with the same intensity at the energy peak. At low energy, both distributions are similar. However, the kappa distribution has a high-energy tail that decreases as a power law.

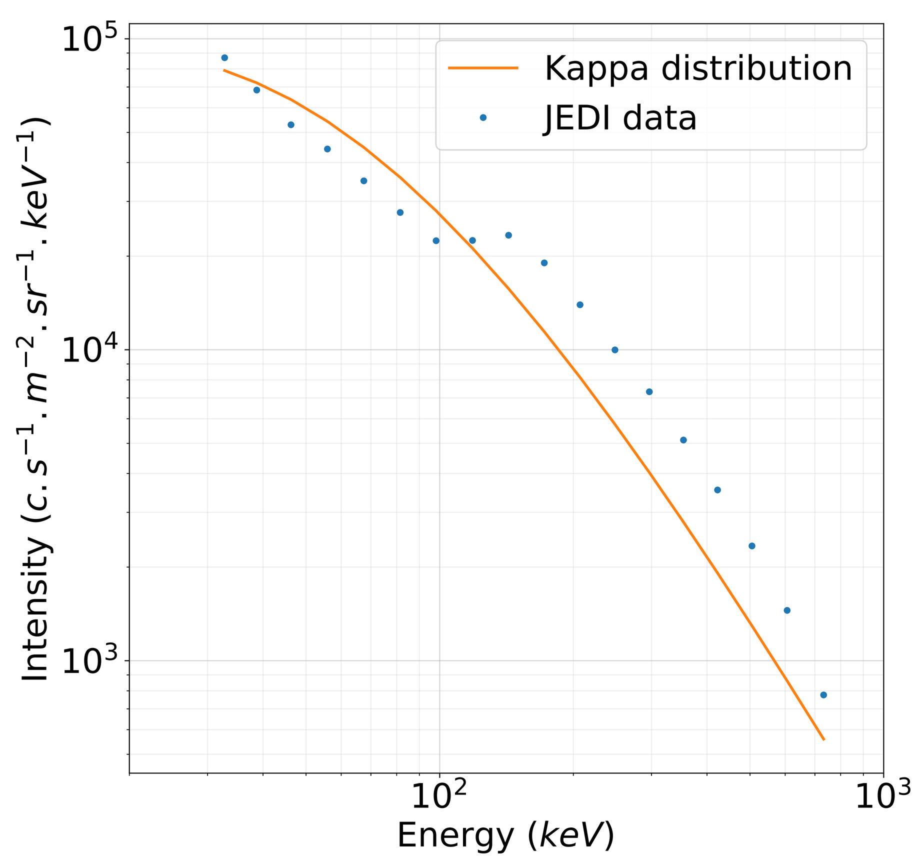

Fig. 2: Kappa distribution displayed over electron distribution measurements. The data points represents the median values of the intensities measured by Juno/JEDI over the main emission during perijoves 1 to 20. With a value of $\kappa = 2.5$, the kappa function appears to be a **good representation** of the electron energy distribution.

5. Results

The curve on Fig. 4 is explained by the existence of a conductance maximum around the mean energy value $E_{\max}$=30 keV (Gérard *et al.*, 2020):

- (1)-(3): Mean energy away from $E_{\max}$ → **enhanced broadband conductance.**
- (2): Mean energy close to $E_{\max}$ → **enhanced mono-energetic conductance.**

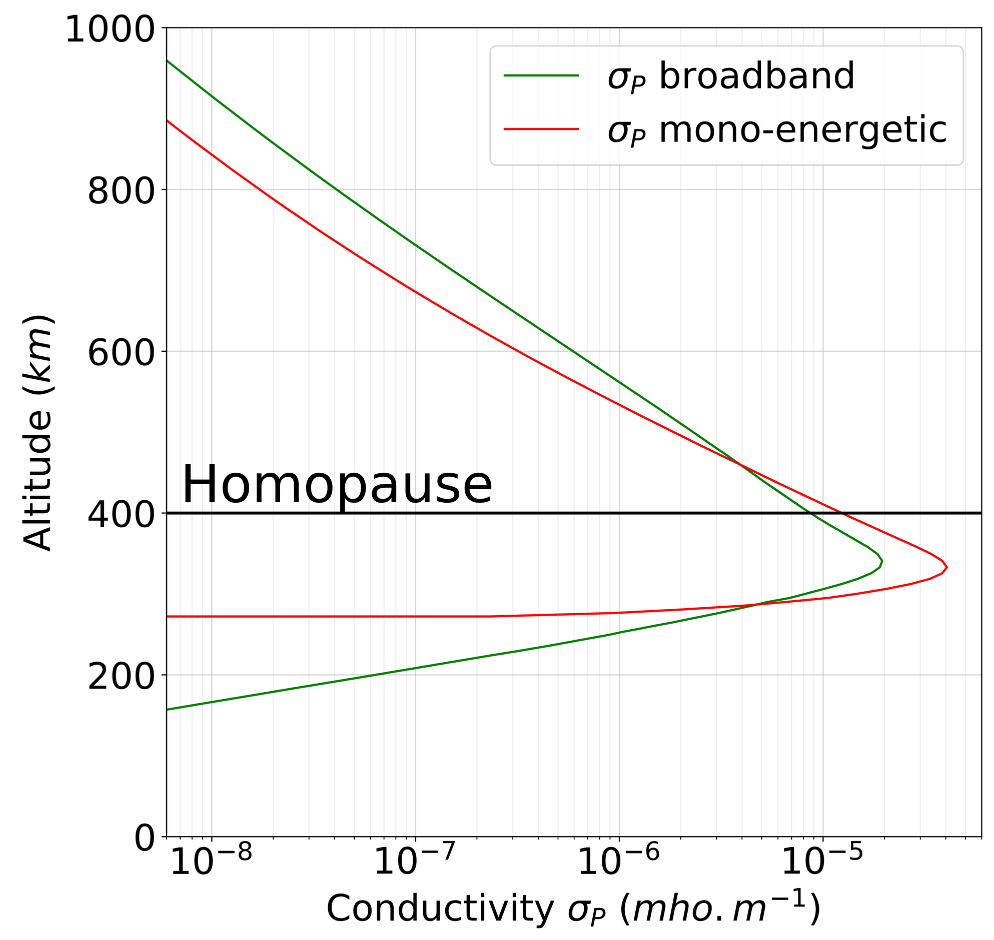

Fig. 3: Comparison between **mono-energetic and broadband vertical profile conductivities** (Q_0=100 mW.m^{-2}, $\langle E \rangle$=40 keV). Understandably, the broadband distribution leads to a broader vertical distribution.

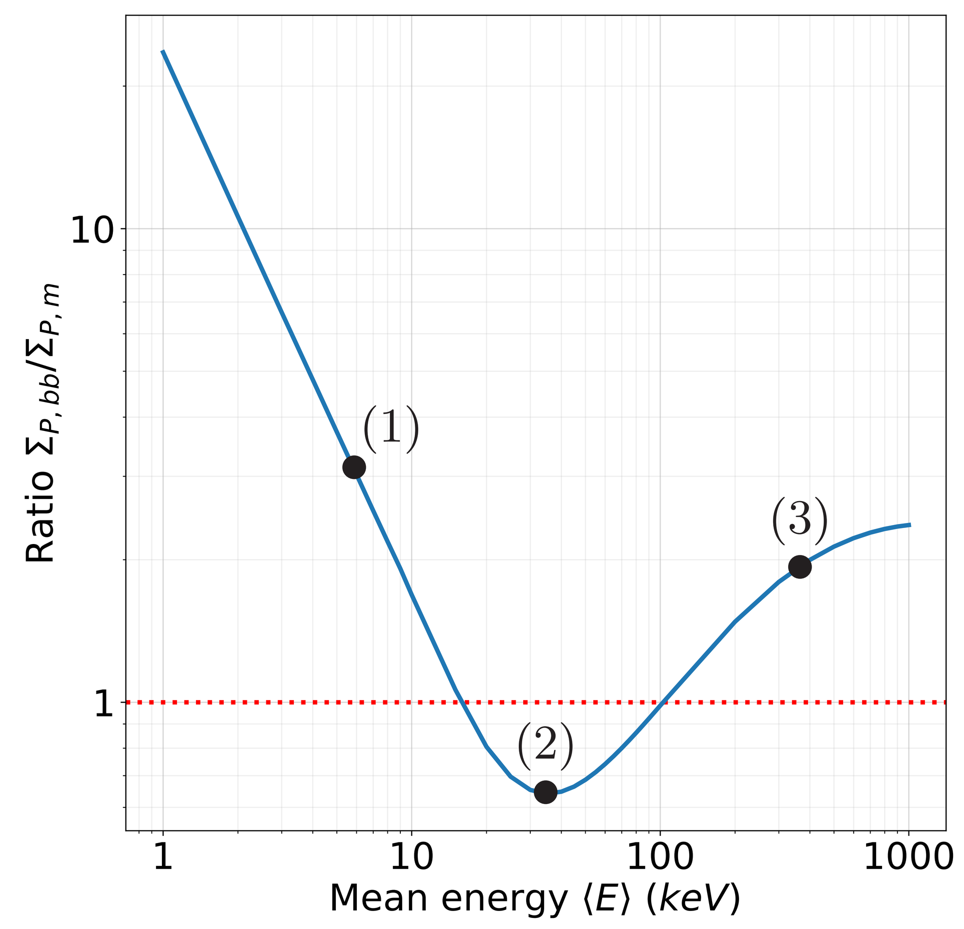

Fig. 4: Ratio between mono-energetic (m) and broadband (bb) conductances as a function of the mean electron energy (Q_0=100 mW.m^{-2}). Even if the ratio greatly depends on the mean energy, it is **almost never equal to 1**.

6. Conclusions

- Compared to a broadband distribution, the conductance deduced from a mono-energetic distribution is either **overestimated by a factor 1.6 in the 15-100 keV range** or **underestimated by a factor of 10 or more outside this range**.
- The next step of this work will be to update the models and conductance maps to better fit the Juno JADE and JEDI observations.

7. References

Coumans, V., Gérard, J.-C., Hubert, B., *et al.* 2002. *J. Geophys. Res Space Phys.*, **107**(A11), SIA5–1–SIA5–12.

Grodent, D., Waite Jr., J.H., & Gérard, J.-C. 2001. *J. Geophys. Res. Space Phys.*, **106**(A7), 12933–12952.

Gérard, J.-C., Gkouvelis, L., Bonfond, B., *et al.* 2020. *J. Geophys. Res Space Phys.*, **125**(8), e2020JA028142.

Hiraki, Y., & Tao, C. 2008. *Ann. Geophys.*, **26**(1), 77–86.

Mauk, B., Haggerty, D., Paranicas, C., *et al.* 2017. *Nature*, **549**(7670), 66–69.

Salveter, A., Saur, J., Clark, G., *et al.* 2022. *J. Geophys. Res. Space Phys.*, **127**(8), e2021JA030224.

Wang, Y., Blanc, M., Louis, C., *et al.* 2021. *J. Geophys. Res. Space Phys.*, **126**(9), e2021JA029469.